



HAL
open science

The chemistry of κ^2 -N,S-chelated Ru(II) complexes with 1,4-diethynylbenzene

Z. Afsan, A. Ahmad, M. Zafar, A. Das, T. Roisnel, S. Ghosh

► To cite this version:

Z. Afsan, A. Ahmad, M. Zafar, A. Das, T. Roisnel, et al.. The chemistry of κ^2 -N,S-chelated Ru(II) complexes with 1,4-diethynylbenzene. Polyhedron, 2022, 227, pp.116120. 10.1016/j.poly.2022.116120 . hal-03830147

HAL Id: hal-03830147

<https://hal.science/hal-03830147>

Submitted on 23 Nov 2022

HAL is a multi-disciplinary open access archive for the deposit and dissemination of scientific research documents, whether they are published or not. The documents may come from teaching and research institutions in France or abroad, or from public or private research centers.

L'archive ouverte pluridisciplinaire **HAL**, est destinée au dépôt et à la diffusion de documents scientifiques de niveau recherche, publiés ou non, émanant des établissements d'enseignement et de recherche français ou étrangers, des laboratoires publics ou privés.

The chemistry of κ^2 -*N,S*-chelated Ru(II) complexes with 1,4-diethynylbenzene

Zeenat Afsan^a, Asif Ahmad^a, Mohammad Zafar^a, Arpita Das^a, Thierry Roisnel^b, Sundargopal Ghosh^{*a}

Abstract: The chemistry of κ^2 -*N,S*-chelated Ru(II) complexes, [Cp*₂RuPPh₃(κ^2 -*N,S*-(NC₇H₄S₂))]₂ (Cp*= η^5 -C₅Me₅), **1a** and [PPh₃{ κ^2 -*N,S*-(NS₂C₇H₄)}Ru{ κ^3 -H,S,S'-H₂B(NC₇H₄S₂)₂}], **1b** has been explored with a terminal alkyne 1,4-diethynylbenzene. For example, the room-temperature reaction of Cp* based κ^2 -*N,S*-chelated Ru(II) species **1a** with 1,4-diethynyl-benzene yielded [RuCp*(κ^1 -*N,S*-C₇H₄NS₂)C₇H₄NS₂-(*E*)-N-C=CHC₈H₅], **2**. On the other hand, although treatment of **1b** with 1,4-diethynyl-benzene at room temperature showed no reactivity, thermolysis led to the formation of two borate complexes, [PPh₃{C₇H₄NS₂-(*E*)-N-C=CHC₈H₅}Ru{ κ^3 -H,S,S'-H₂B(C₇H₄NS₂)₂}], **3** and [PPh₃(κ^2 -*N,S*-C₇H₄NS₂) Ru{ κ^3 -S,S',S''-HB(C₇H₄NS₂)₃}], **4**, albeit in poor yields. Both the Ru(II) species **2** and **3** contain a five-membered ruthenacycle with an exocyclic C=C moiety attached to carbon atom. In complex **4**, the ruthenium center is stabilized by hydrotrisborate, phosphine, and hemilabile one *N,S*-chelating ligand. The key feature of **4** is the coordination of the boron atom to the metal center through a common sulphur atom of the 2-mercaptobenzothiazole ligand. Characterization of these Ru(II) species has been carried out by various spectroscopic techniques and single-crystal X-ray diffraction analysis for **4**. In addition, Density Functional Theory (DFT) calculations were further performed to provide insight into the bonding and electronic structures of these complexes.

Keywords: Ruthenium, hemilabile, borate, insertion, terminal alkyne

^a Department of Chemistry, Indian Institute of Technology Madras, Chennai 600 036, India.

^b Univ Rennes, CNRS, Institut des Sciences Chimiques de Rennes, UMR 6226, F-35042 Rennes, France.

*Corresponding Author. Phone: (+91) 44 2257 4230; Fax: (+91) 44 2257 4202.

E-mail address: sghosh@iitm.ac.in

1. Introduction

The synthesis and chemistry of transition-metal-based complexes having functional ligands continue to be the area of intense research in organometallic chemistry over the past few decades. Typically, the design of functional ligands is an important strategy to achieve various structural motifs adopted by transition metal complexes [1,2]. These ligands actively participate to tune the coordination mode of the metal and thus facilitates bond activation processes. For instance, Sabo-Etienne and group have reported a phosphinobenzyl-(amino) borane ligand-based ruthenium complex with two adjacent B–H and C–H agostic interactions and affords selective B–H, C–H, and B–C bond activation [3]. Recently, we have explored versatile coordination modes of mercaptobenzothiazolyl/pyridyl borate ligands at the ruthenium center that are stabilized by 1,3-*N,S* donor ligand either in chelating (κ^2 -*N,S*) or bridging (μ^2 -*N,S*/ μ^1 -*S*) coordination modes [4,5]. In fact, these 1,3-*N,S* chelated ligands have shown potential hemilabile character to provide the coordinative unsaturation at the metal center for further functionalization and access to various functional groups with different steric and electronic properties.

The activation of C–H bond mediated by transition-metal complexes with regioselective and site-specific functionalization has witnessed much prominence in the recent past. In regard to this, various research groups have extensively studied the reactivity of different transition metal-based complexes towards unsaturated terminal alkynes [6,7]. For example, Martín and co-workers have carried out the activation of an alkyne C–H bond by ruthenium complex [Ru(Cl)H(CO)(PiPr₃)₂] (Chart 1, I) [8]. Likewise, Oldenhof *et al.* have reported intermolecular C–H activation of terminal alkynes by Sulfonamidophosphine ligands (coined as METAMORPhos) in the coordination sphere of an Ir-METAMORPhos piano-stool complex (Chart 1, II) [9]. Schafer and co-workers studied insertion of terminal alkynes into the Ir–O bond of 1,3-*N,O*-chelated phosphoramidate Cp*Ir(III) complex, [Cp*Ir(κ^2 -*N,O*-2,6-Me₂C₆H₃(N)P(O)(OEt)₂][BAr^F₄] (ArF = 3,5-(CF₃)₂C₆H₃) (Chart 1, III) [10]. More recently, Castarlenas and group reported an alkyne inserted *N,O*-chelated pyridonato rhodium complex, Rh{ κ^2 -*O,N*-(Opy)} { η^2 -H₂C=C(Mes)-C≡C(Mes)}(IPr), generated upon catalytic alkyne dimerization, where the C–C and C–heteroatom bond formation occur by C–H activation (Chart 1, IV) [11].

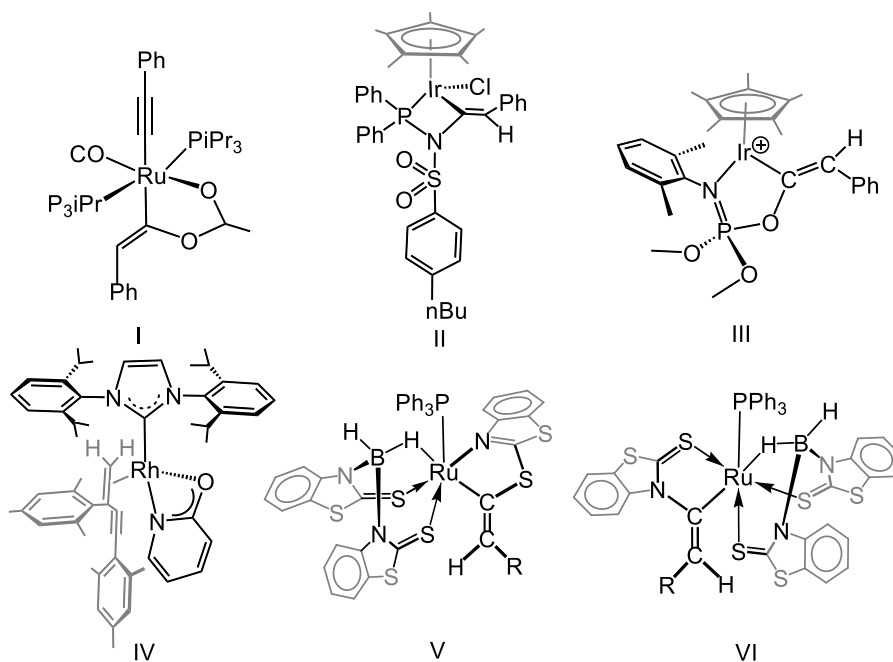


Chart 1. Examples of C–H bond activation of terminal alkynes by different transition metal complexes.

In continuation of our recent studies, we have exploited the reactivity of transition metal boron and borate complexes with different alkynes [12–15]. For example, thermolysis of Cp* based ruthenium borate complex $[\text{Cp}^*\text{Ru}(\text{PPh}_2(\text{CH}_2)\text{PPh}_2)\text{BH}_2(\text{C}_7\text{H}_4\text{NS}_2)_2]$ ($\text{Cp}^* = \eta^5\text{-C}_5\text{Me}_5$), upon treatment with different terminal alkynes generated η^2 -vinylborane complexes *via* hydroboration reaction [16]. More recently, we have investigated the reactivity of κ^2 -*N,S*-chelated ruthenacycle borate complexes towards different alkynes [4]. Interestingly, the borate complexes showed remarkable C–H activation of terminal alkynes that formed five-membered ruthenacycles with an exocyclic C–C double bond. They are believed to be generated upon insertion of alkynes into both Ru–N and Ru–S bond of the hemilabile κ^2 -*N,S*-chelating ruthenacycle (Scheme 1, V–VI). These findings encouraged us to further investigate the role of terminal alkynyl with an aromatic spacer. The synthetic tailoring of transition metal complexes with bridging alkynyl aromatic spacer units has shown remarkable abilities in providing strong electronic interaction between the two inaccessible redox-active metal centers [17–20]. Therefore, with the objective to synthesize “alkyne-bridged” ruthenium complexes with aromatic spacer units and to probe the role of hemilabile *N,S*-chelated ruthenacycle, herein, we have explored the reactivity of Cp* based κ^2 -

N,S-chelated Ru(II), **1a** [21] and κ^2 -*N,S*-chelated Ru(II) borate complexes, **1b** [4] towards 1,4-diethynylbenzene.

2. Experimental details

2.1. General methods and instrumentation:

All the syntheses were conducted under a dry argon atmosphere utilizing standard Schlenk line and glovebox techniques. Solvents (toluene, hexane, and tetrahydrofuran) were distilled by Sodium/benzo-phenoneketyl, and dichloromethane was dried over calcium hydride under argon before use. Complexes [Cp*RuPPh₃(κ^2 -*N,S*-(NC₇H₄S₂))] [21], **1a**; [PPh₃{ κ^2 -*N,S*-(NS₂C₇H₄)}Ru{ κ^3 -*H,S,S'*-H₂B(NC₇H₄S₂)₂}] [4], **1b** and 1,4-diethynylbenzene [22] were synthesized using procedure reported earlier. Thin-layer chromatography was performed on 250 μ m diameter aluminium-supported silica gel TLC plates (Merck TLC plates). The external reference for the ¹¹B{¹H} NMR spectroscopy, [Bu₄N][(B₃H₈)] was prepared as per the reported method [23]. NMR spectra were recorded on Bruker 400 and 500 MHz instruments. The residual solvent protons were used as reference (δ , ppm, CDCl₃, 7.26), whereas for ¹¹B NMR spectra, a sealed tube with [Bu₄N][(B₃H₈)] in Benzene-*d*₆ (δ_B , ppm, -30.07) was utilized as an external reference. High-resolution ESI-MS were recorded on Bruker Micro-TOF-II mass spectrometer in ESI ionization mode. Infrared spectra were obtained on a Jasco FT/IR-1400 spectrometer.

2.2. Synthesis of **2**

In a flame-dried Schlenk tube, in-situ generated **1a** (200 mg, 0.300 mmol) in dry toluene (10 mL) was treated with one equivalent of 1,4-diethynylbenzene (39 mg, 0.300 mmol) at room temperature for 12 h. The solvent was evaporated under vacuum, and the residue was extracted into CH₂Cl₂/hexane and passed through celite. After removing solvents, the chromatographic workup of the residue was done using TLC plates. Further, the elution with a mixture of CH₂Cl₂/hexane (80/20 v/v) yielded orange solid **2** (12 mg, 6%) [24].

2: MS (ESI⁺): *m/z* calculated for [C₃₄H₃₀N₂RuS₄ + H]⁺: 698.0496 found 698.0886; ¹H NMR (400 MHz, CDCl₃, 22 °C): δ = 8.25 (br, 1H, N-H), 7.74 (d, *J* = 7.6 Hz, 1H, Ar_(mbz)), 7.70 (s, 1H, Ar_(mbz)), 7.68 – 7.65 (m, 2H, Ar_(mbz)), 7.64 – 7.46 (m, 2H, Ar_(mbz)), 7.49 – 7.44 (m, 4H, Ar), 7.17 (d, *J* = 8.0

Hz, 1H, Ar_(mbz)), 7.13 (d, J = 8.4 Hz, 1H, Ar_(mbz)), 7.00 (s, 1H, CHC₈H₅), 3.49 (s, 1H, C≡CH), 1.60 (s, 15H, C₅Me₅).

2.2. Synthesis of **3** and **4**:

In a flame-dried Schlenk tube, a solution of **1b** (200 mg, 0.228 mmol) in 10 mL dry toluene was treated with one equivalent of 1,4-diethynylbenzene (29 mg, 0.228 mmol) under argon and the reaction mixture was stirred for 24 h at 80°C. The solvent was dried under vacuum, the residue was extracted in a hexane/CH₂Cl₂ mixture and further passed through celite. After removing the solvent, the chromatographic workup using TLC plates of the residue was performed. Elution with hexane/CH₂Cl₂ (30:70 v/v) yielded yellow solid **3** (16 mg, 8%) and red solid **4** (24 mg, 12%) [24].

3: MS (ESI⁺): *m/z* calculated for [C₄₉H₃₅BN₃PRuS₆]⁺: 1001.0041, found 1001.0084; ¹¹B{¹H} NMR (160 MHz, CDCl₃, 22 °C): δ = -4.4 ppm (br, B); ³¹P{¹H} NMR (202 MHz, CDCl₃, 22 °C): δ = 43.3 ppm; ¹H NMR (500 MHz, CDCl₃, 22 °C): δ = 8.23 (d, J = 8.4 Hz, 1H, Ar_(mbz)), 7.51 (m, 7H, Ar_(mbz)), 7.40 – 7.37 (m, 2H, Ar_(mbz)), 7.32 (m, 2H, Ar_(mbz)), 7.31 – 7.29 (m, 4H, Ar), 7.22 – 7.18 (m, 2H, Ar), 7.16 – 7.14 (m, 2H, Ar), 7.11 (m, 4H, Ar), 7.04 (m, 6H, Ar), 6.82 – 6.77 (m, 1H, Ar_(mbz)), 6.75 (s, 1H, CHC₈H₅), 4.61 (br, 1H, B-H_i), 3.05 (s, 1H, C≡CH), -6.29 ppm (br, 1H, Ru-H-B); IR (CH₂Cl₂, cm⁻¹): ν̄ = 2403 (B-H_i), 2299 (B-H_b).

4: MS (ESI⁺): *m/z* calculated for [C₄₆H₃₃BPN₄RuS₈]⁺: 1040.9355, found 1040.9357; ¹¹B{¹H} NMR (160 MHz, CDCl₃, 22 °C): δ = -7.6 ppm (br, B); ³¹P{¹H} NMR (202 MHz, CDCl₃, 22 °C): δ = 47.7 ppm; ¹H NMR (500 MHz, CDCl₃, 22 °C): δ = 7.95 (d, J = 8.3, 1H Ar_(mbz)), 7.86 (d, J = 8.1, 1H Ar_(mbz)), 7.80 (d, J = 8.3 1H, Ar_(mbz)), 7.65 (d, J = 8.2, 1H, Ar_(mbz)), 7.40 (m, 10H, Ar), 7.31 (m, 4H, Ar), 7.12 (m, 1H Ar_(mbz)), 7.04 – 7.03 (m, 4H, Ar_(mbz)), 6.94 – 6.93 (m, 2H, Ar_(mbz)), 6.84 – 6.82 (m, 6H, Ar_(mbz)), 4.86 (br, 1H B-H_i); ¹³C{¹H} NMR (126 MHz, CDCl₃, 22 °C): δ = 115.2, 116.0, 120.9, 121.7 (C=C), 122.10, 122.9, 124.4, 124.6, 126.8, 127.6, 129.3, 130.2, 135.2 (C₆H₅), 145.1, 145.2 (C=N), 198.44 ppm (C=S); IR (CH₂Cl₂, cm⁻¹): ν̄ = 2408 (B-H_i).

2.3. Computational details

All the molecules have been optimized in gaseous phase (no solvent effect) using Gaussian 09 [25] program using the functional B3LYP [26-28] in conjunction with def2-SVP [29] basis set from Basis Set Exchange Library [30]. The optimized geometries were in minima energy on the potential

energy hypersurface diagram, confirming the absence of any imaginary frequencies. We have computed the ^1H and ^{11}B NMR chemical shifts at B3LYP/GIAO method [31-33]. TMS (SiMe_4) was used as internal standard for ^1H NMR calculations and the ^{11}B NMR chemical shifts were considered comparative to $[\text{B}_2\text{H}_6]$ and converted to typical $[\text{BF}_3\cdot\text{OEt}_2]$ scale utilizing the experimental $\delta(^{11}\text{B})$ value of B_2H_6 (16.6 ppm) [34]. Natural bonding analysis was carried out using the natural bond orbital (NBO) 6.0 version of program [35]. Wiberg bond indices (WBI) were derived using NBO analysis [36]. The topological parameters, Laplacian electronic distribution, and electron density were analysed with the quantum theory of atoms in molecules (QTAIM) [37-39] using Multiwfn Version 3.8 package [40]. Further, Chemcraft was used to generate the optimized structures and orbital plots [41].

2.4. X-ray Structure Determination:

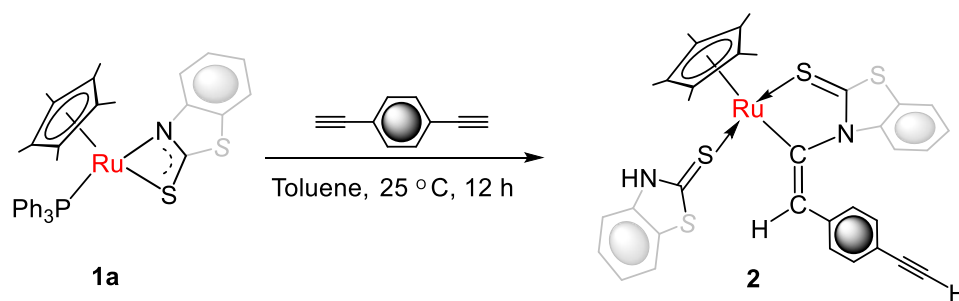
Crystals of **4** suitable for X-ray diffraction studies were obtained upon slow diffusion of a hexane/ CH_2Cl_2 solution. The crystal data of **4** were obtained using a D8 VENTURE Bruker SC diffractometer with graphite monochromated Mo- $\text{K}\alpha$ ($\lambda = 0.71073 \text{ \AA}$) radiation at 200(2) K. The structure was solved by SIR97 [42] and further refined with SHELXL-2014, SHELXL-2017 and SHELXL-2018, [43]. Olex2 was used to draw the molecular structure [44]. All non-hydrogen atoms were refined with anisotropic displacement parameters, and the hydrogen atoms could be located in the difference Fourier map. Crystallographic data were deposited with the Cambridge Crystallographic Data Center as supplementary publication no. CCDC-2177348 (**4**). These data can be obtained from the Cambridge Crystallographic Data Center free of charge via www.ccdc.cam.ac.uk/data_request/cif.

Crystal data for **4**: $\text{C}_{47}\text{H}_{34}\text{BN}_4\text{PRuS}_8$, $M_r = 1125.01$, triclinic, space group P-1, $a = 11.2184(15) \text{ \AA}$, $b = 13.3572(16) \text{ \AA}$, $c = 16.698(2) \text{ \AA}$, $\alpha = 106.101(5)$, $\beta = 101.690(5)^\circ$, $\gamma = 90.424(5)^\circ$, $V = 2348.7(5) \text{ \AA}^3$, $Z = 2$, $\rho_{\text{calcd}} = 1.591 \text{ g/cm}^3$, $\mu = 0.878 \text{ mm}^{-1}$, $F(000) = 1140$, $R_1 = 0.0825$, $wR_2 = 0.1940$, 10509 independent reflections [$2\theta \leq 55.168^\circ$] and 409 parameters.

2. Results and Discussion

3.1. Reactivity of **1a** with 1,4-diethynylbenzene

As shown in Scheme 1, the room-temperature reaction of **1a** with 1,4-diethynylbenzene in toluene yielded ruthenium alkenyl complex $[\{\text{RuCp}^*(\kappa^1\text{-N-C}_7\text{H}_4\text{NS}_2)\text{C}_7\text{H}_4\text{NS}_2\text{-(E)-N-C=CHC}_8\text{H}_5\}]$, **2**. Complex **2** might have been generated upon the insertion of terminal alkyne, 1,4-diethynylbenzene into the Ru–N bond of hemilabile $\kappa^2\text{-N,S}$ -chelated ligand resulting in a five-membered ruthenacycle. The detailed mechanism for the formation of such type of insertion has been described in our earlier work [4]. The chromatographic separation allowed us to separate **2** as orange solid in very low yield. This was characterized by multinuclear NMR, and IR spectroscopy. Although we were unable to get the X-ray structure for this species, all the spectroscopic data along with mass spectrometric data support the composition and structure as shown in Scheme 1. The ^1H chemical shift values for **2** suggest the presence of both olefinic and acetylenic protons along with Cp* and benzothiazolyl ligands (Figure S4). The $^{31}\text{P}\{^1\text{H}\}$ NMR shows the absence of ^{31}P chemical shift. The mass spectrum of **2** depicts a molecular ion peak at m/z 698.0187.



Scheme 1. Synthesis of the Cp* based ruthenium alkenyl complex **2**.

Computational density functional theory (DFT) and natural bond orbital (NBO) analysis have been implemented to acquire some perception on the electronic structure and nature of bonding in complex **2**. The selected bond lengths of the ground state optimized structure (Figure 1a) are provided in Table S1. The ^1H chemical shifts calculated by the gauge-including atomic orbitals (GIAOs) method are in agreement with experimental values (Table S2). The molecular orbital (MO) analysis of **2** shows a HOMO–LUMO gap of 2.20 eV. The HOMO–5 mainly involves inserted alkenyl moiety suggesting the presence of the C=C bond (Figure 1b). This was further supported by the Wiberg bond indices (WBI) value obtained by NBO analyses (1.73, Figure 1c and Table S1). In addition, the Laplacian electron density plot of **2** obtained from the quantum theory of atoms and molecules (QTAIM) analysis displays bond critical points (BCPs) in the Ru–C–C plane, similar to the electron density for BCP of the C=C bond (Figure 1d). The bond properties of **2** at the selected

BCPs are provided in Table S5. In addition, the ring critical point (RCP) in **2** suggests the presence of a five-membered RuNCSC ring system (Figure S13a).

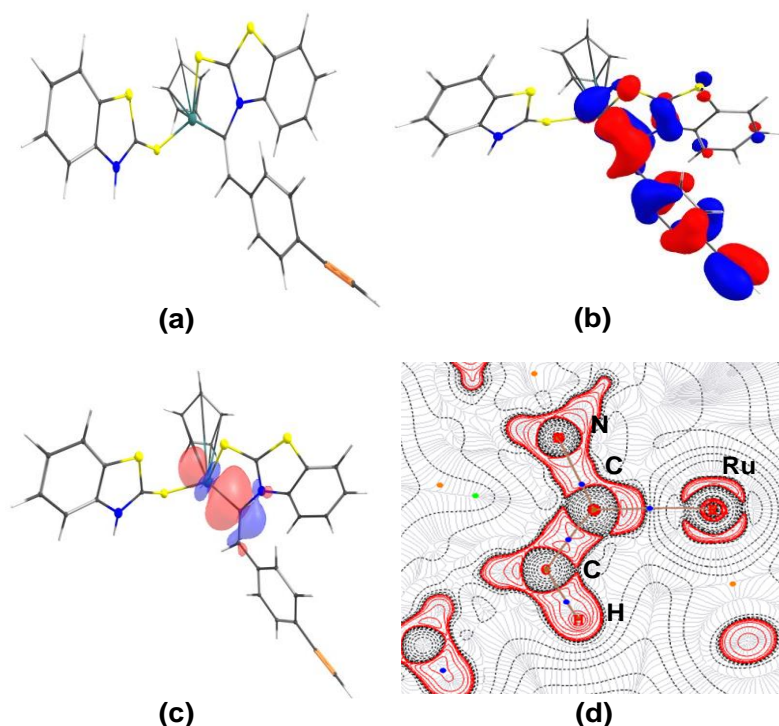


Figure 1. (a) Optimised geometry of **2**; (b) HOMO-5 orbital of **2** involving C=C bonding interaction; (c) Natural bond orbital interaction between Ru-C-C in **2** (contour value: ± 0.036 [e/bohr^3] $^{1/2}$); and (d) the Laplacian electron density along Ru-C-C plane of **2**. Areas of charge concentration [$\nabla^2\rho(r)<0$] are shown by red lines and regions of charge depletion [$\nabla^2\rho(r)>0$] are indicated by black lines. The solid brown lines indicate bond paths, and blue spheres represent bond-critical points.

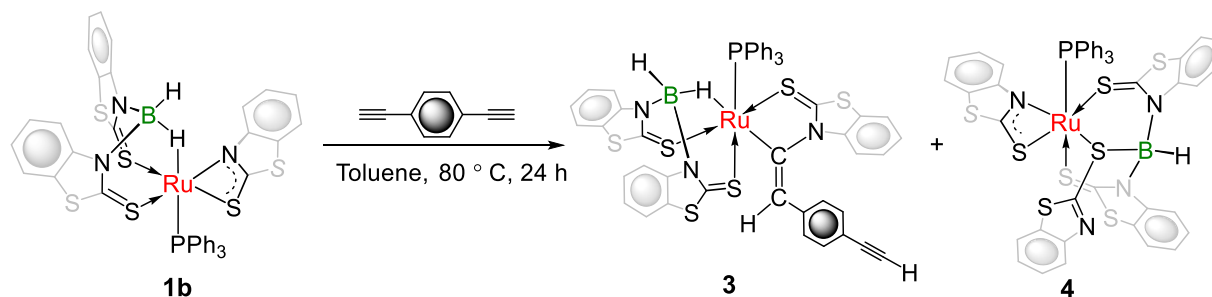
3.2. Reactivity of **1b** with 1,4-diethynylbenzene

As shown in Scheme 2, thermolysis of κ^2 -*N,S*-chelating Ru(II) borate complex **1b** with 1,4-diethynylbenzene in toluene led to the formation of two complexes **3** and **4**, albeit in low yields. After chromatographic purification using TLC, we have isolated them in pure form and characterized as ruthenium alkenyl species [$\text{PPh}_3\{\text{C}_7\text{H}_4\text{NS}_2\text{-}(E)\text{-N-C=CHC}_8\text{H}_5\}\text{Ru}\{\kappa^3\text{-H,S,S}'\text{-H}_2\text{B}(\text{C}_7\text{H}_4\text{NS}_2)_3\}$], **3** and Ru(II) borate species [$\text{PPh}_3(\kappa^2\text{-N,S-C}_7\text{H}_4\text{NS}_2)\text{Ru}\{\kappa^3\text{-S,S}',\text{S}''\text{-HB}(\text{C}_7\text{H}_4\text{NS}_2)_2\}$] **4**. Both the complexes were characterized by multinuclear NMR and IR

spectroscopy, mass spectrometry, and a single crystal X-ray diffraction study for one of the species **4**.

The $^{11}\text{B}\{^1\text{H}\}$ spectrum of **3** shows a sharp peak at $\delta = -4.4$ ppm that confirms the presence of a single boron environment. The $^{31}\text{P}\{^1\text{H}\}$ NMR spectrum of **3** shows a peak at 43.3 ppm for PPh_3 ligand. In addition to the presence of mercaptobenzothiazolyl and phosphine ligand, the ^1H NMR spectrum of **3** displays a peak $\delta = 4.61$ ppm that could be attributed to the B-H_t proton. The ^1H NMR spectrum of **3** depicts an upfielded chemical shift at $\delta = -6.29$ ppm, assignable to the Ru-H-B proton. Moreover, ^1H NMR chemical shift values suggest the presence of olefinic and acetylenic proton (Figure S5). The IR spectrum of **3** shows bands at 2299 and 2403 cm^{-1} suggestive of Ru-H-B and B-H_t stretching frequencies, respectively. The mass spectrometric data shows a peak at m/z 1001.0045 for **3** which corresponds to the formulation $\text{C}_{49}\text{H}_{35}\text{BN}_3\text{PRuS}_6$. All the spectroscopic data along with mass spectrometric data are evident for the formation of the alkyne inserted ruthenium alkenyl borate complex **3** as shown in Scheme 2.

Along with the formation of Ru(II) alkenyl species **3**, complex **4** was also isolated in the same reaction with 24% yield. The $^{11}\text{B}\{^1\text{H}\}$ spectrum of **4** displays a single peak at $\delta = -7.6$ ppm for a single boron atom and the $^{31}\text{P}\{^1\text{H}\}$ NMR spectrum features a singlet at $\delta = 47.7$ ppm. The ^1H NMR spectrum of **4** provides a chemical shift for B-H_t proton at $\delta = 4.86$ ppm. In addition, the spectrum reveals the presence of two different environments of benzothiazole units. The ^{13}C NMR spectrum peaks confirm the presence of benzothiazole ligands. The IR spectrum displays a band at 2408 cm^{-1} assignable to the B-H_t bond. The mass spectrum of **4** shows a molecular-ion peak at m/z 1040.9332. Although all of the spectroscopic data suggest **4** to be a new Ru -borate species, the unambiguous molecular structure was confirmed by the X-ray diffraction study.



Scheme 2. Synthesis of the ruthenium borate complexes **3** and **4**.

The single-crystal x-ray diffraction analysis was carried out to illustrate the geometry and bonding of **4**. Single crystal of **4** suitable for X-ray diffraction analysis was obtained from the slow diffusion of a hexane-CH₂Cl₂ solution at -5 °C. Complex **4** crystallizes in the triclinic system with P-1 space group. As shown in Figure 2, the molecular structure of **4** elucidates the coordination of a 2-mercaptobenzothiazole ligand bridged between the boron and metal center. The ruthenium center in **4** adopts a distorted octahedral geometry, stabilized by triphenylphosphine, hydrotrisborate and hemilabile *N,S*-chelating ligands, where the equatorial plane is occupied by one nitrogen and three sulphur atoms (S-S-S-N) of hydrotrisborate and hemilabile *N,S*-chelating ligands alongside the sulphur atom of hydrotrisborate ligand trans to phosphine moiety in the axial position. The *N,S*-chelating ligand engenders a four-membered ring (S-Ru-N) exhibiting a bite angle of 67.45(16)° comparable to that of [(PPh₃)₂Ru(*N,S*-mbz)₂] (67.295(11)°) [45]. The B53-S21 bond distance of 1.912(8) Å is within the range of the single B-S distance reported for borate-thiolate species [46]. Moreover, the observed Ru1-S1 distance of 2.4614(18) Å in **4** is notably longer than the Ru1-S21, Ru1-S11, and Ru1-S31 distances [2.313(17) Å, 2.367(16) Å and 2.393(17) Å respectively], that are comparable to [RuH(CO)(PPh₃) $\{\kappa^3$ -H,S,S-HB(mt)₃] (mt = methimazolyl) and [(HMB)Ru(9S₃)] (HMB = η⁶-C₆Me₆ and 9S₃ = trithiacyclononane) [47,48]. In addition, Ru1-S31 distance trans to the PPh₃ is found longer than the other equatorial Ru-S distance of the hydrotrisborate ligand. However, Ru1-S21 bond is comparatively shorter, suggesting stronger interaction of the 2-mercaptobenzothiazole ligand with the metal center. The observed dissimilar Ru-S bond distances in **4** could be due to the presence of different sulphur centers. Complex **4** differs from other transition metal borate complexes with soft scorpionate ligands owing to the coordination of three sulphur donors to the metal center. Interestingly, two mercaptobenzothiazolyl ligands are bound with the metal and boron atoms through sulphur and nitrogen atoms, respectively. Complex **4** shows the absence of any direct Ru-B bond or agostic interaction between ruthenium and the B-H bond; nevertheless, metal and the boron center are bridged through a common sulphur atom of the dangling 2-mercaptobenzothiazole ligand. Therefore, boron atom is tetrahedrally coordinated where one of the coordination sites is satisfied through the sulphur atom alongside two nitrogen atoms of 2-mercaptobenzthiazole.

Various transition metal tris(methimazolyl)-borate complexes have been reported, where the metal center coordinates to the ligand through soft sulphur, while the boron is bound to the hard

nitrogen center [49-51]. Bailey and co-workers reported a tris(methimazolyl)hydroborate Ru(II) complex [(Tm)RuCl(DMSO)₂], {Where Tm = tris(methimazolyl)hydroborate} from the reaction of [RuCl₂(DMSO)₄] with tris(methimazolyl)hydroborate ligand in which ruthenium centre is coordinated with the sulphur atom of methimazolyl moiety and boron is attached with nitrogen center of the ligand [50]. Another notable hydrotrisborate species [Cp*₂RuBH{2-mercaptobenzthiazol}₃] was generated from the reaction of [Cp*₂RuCl₂]₂ (Cp* = η⁵-C₅Me₅) with dihydrobis(2-mercapto-benzthiazolyl)borate, where one of the 2-mercaptobenzothiazole ligand connects to the ruthenium metal and the boron center through a common sulphur atom [52].

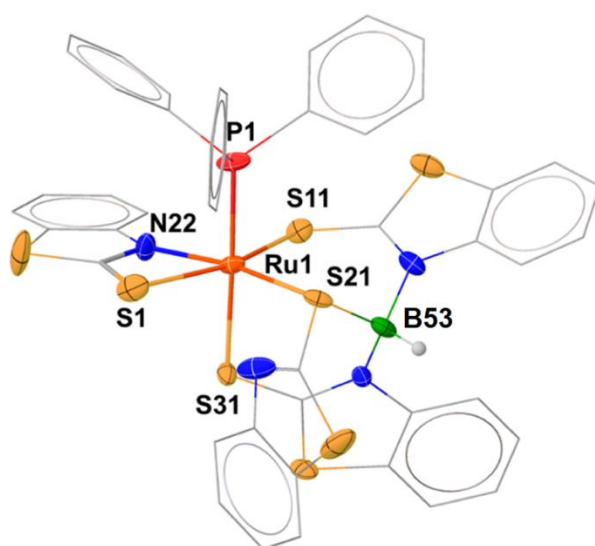


Figure 2. Molecular structure of **4**. Selected bond lengths (Å) and angles (°): Ru1–S21 2.313(17), Ru1–S11 2.367(16), Ru1–S31 2.393(17), Ru1–S1 2.461(18), Ru1–N22 2.122(6), Ru1–P1 2.307(18), B53–S21 1.912(8), N22–Ru1–S1 67.45(16), N22–Ru1–S31 86.53(17), N22–Ru1–S11 92.41(16), P1–Ru1–S11 91.81(6).

DFT calculations have been performed to account for the bonding and the nature of interaction in complexes **3** and **4**. The bond parameters and the ¹H and ¹¹B computed chemical shifts for **3** and **4** closely resembled the experimental findings (Tables S1 and S2). The calculated energy values for **3** and **4**, given in Table S3, show the formation of complexes. The MO analysis shows a larger HOMO–LUMO gap for **3** (3.204 eV) than **2**, suggesting higher stability of **3**. The HOMO–1 orbital of **3** mainly involves inserted alkenyl moiety (Figure 3a). Moreover, the contour-line map for **3** in the Ru–C–C plane provides a comparable electron density at bond critical points BCP of the C–C

double bond (Figure 3c). The NBO results indicate the significant Ru–H–B bonding interactions in **3** with a WBI value of 0.18. The natural charge on the phosphorous atom in **3** (1.213) is positive, whereas the Ru atom (-0.849) exhibits a negative charge, suggestive of the charge transfer from phosphorous to the ruthenium center. Further, the transfer of electrons was supported by the increase in the natural valence population for Ru with a subsequent decrease over phosphorous atom (Table S4). In addition, the contour plot of **3** displays BCPs between Ru–H and B–H bonds in the Ru–H–B plane with $\nabla^2\rho(r)$ and $H(r)$ of 0.270 a.u. and -0.111 a.u., respectively (Figure S13c).

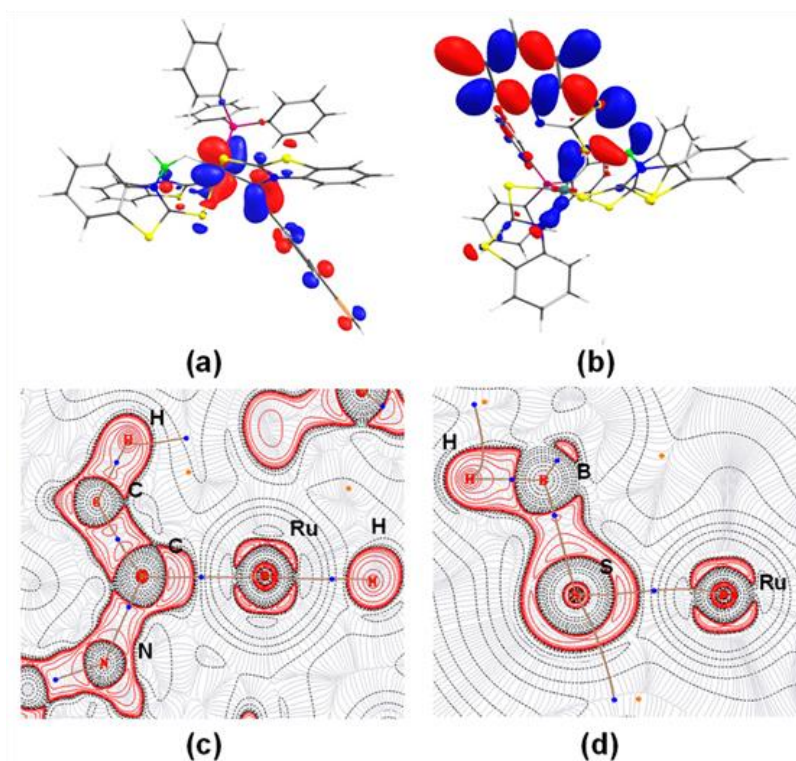


Figure 3. (a) HOMO–1 orbital for **3** involving C=C bonding interaction; (b) HOMO–38 orbital for **3** involving Ru1, S21, and boron atoms in **4** (contour value: ± 0.036 [e/bohr^3] $^{1/2}$); (c) and (d) the Laplacian of the electron density along the Ru–C–C and Ru–S–B plane of **3** and **4**, respectively. The solid brown lines are bond paths, while the blue indicates the bond-critical points. Areas of charge depletion [$\nabla^2\rho(r) < 0$] are shown by red lines, whereas areas of charge concentration [$\nabla^2\rho(r) > 0$] are indicated by black lines.

The MO analysis suggests that HOMO of **4** comprises of d-orbitals of ruthenium, whereas the ligand orbitals contribute more to LUMO. The HOMO–38 depicts the bonding interaction between

Ru1, S21, and boron atoms (Figure 3b), whereas LUMO+2 mainly involves the 2-mercaptobenzthiazole ligand (Figure S12). Further, the WBI values of Ru–N, Ru–S, and B–N bonds illustrate strong bonding interactions in **4** (Figure 3b, Table S1). The contour-line map of the Laplacian of the electron density of **3** shows BCPs between Ru–S and B–S bonds along the Ru–S–B plane (Figure 3d) with Laplacian of the electron density ($\nabla^2\rho(r)$) and energy density ($H(r)$) of 0.223 a.u. and -0.102 a.u., respectively. Furthermore, the presence of RCP in **4** indicates the existence of a four-membered RuNCS ring (Figure S13d).

4. Conclusions

In summary, the reactivity of κ^2 -*N,S*-chelated Ru(II) species having comprising Cp* as well as borate unit has been carried out with terminal alkyne, 1,4-diethynylbenzene. We have isolated and characterized ruthenium alkenyl complexes **2** and **3** which are formed upon insertion of activated alkyne, 1,4-diethynylbenzene into Ru–N bond of the hemilabile κ^2 -*N,S*-chelated ring system with exocyclic C=C bond. In addition, a ruthenium borate species **4** has been isolated and structurally characterized which is stabilized by hydrotrisborate, phosphine and *N,S*-chelating ligand. The significance of species **4** is the coordination around boron through a common sulphur atom of dangling 2-mercaptobenzothiazole ligand. The computational DFT calculations further provided insight into the bonding and electronic structures of these complexes.

Acknowledgments

This work was supported by the Council of Scientific and Industrial Research (CSIR) (Scheme No. 01(3055)/21/EMR-II), New Delhi, India. Z. A. is thankful to IIT Madras for the institute postdoctoral fellowship. A. A. thanks CSIR and M. Z. thanks IIT Madras for research fellowship. The computational facility of IIT Madras is gratefully acknowledged.

Notes and references

- [1] P. Braunstein, J. Organomet. Chem. 689 (2004) 3953–3967.
- [2] R. H. Crabtree, New J. Chem. 35 (20011) 18–23.
- [3] A. Cassen, Y. Gloaguen, L. Vendier, C. Duhayon, A. Poblador-Bahamonde, C. Raynaud, E. Clot, G.

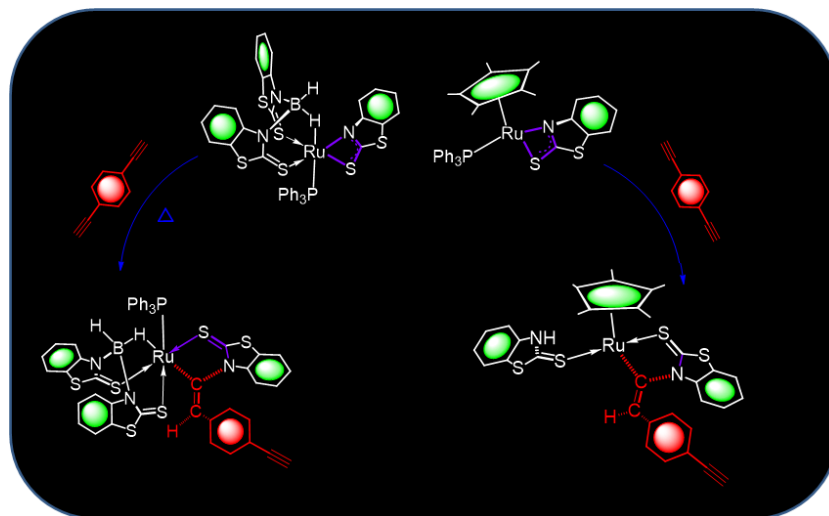
- Alcaraz, S. Sabo-Etienne, *Angew. Chem. Int. Ed.* 53 (2014) 7569–7573.
- [4] M. Zafar, R. Ramalakshmi, K. Pathak, A. Ahmad, T. Roisnel, S. Ghosh, *Chem. – A Eur. J.* 25 (2019) 13537–13546.
- [5] M. Zafar, A. Ahmad, S. Saha, R. Ramalakshmi, T. Roisnel, S. Ghosh, *Chem. Sci.* (2022) Advance Article.
- [6] D.G. Johnson, J.M. Lynam, J.M. Slattery, C.E. Welby, *Dalton. Trans.* 39 (2010) 10432–10441.
- [7] J. Guihaumé, S. Halbert, O. Eisenstein, R.N. Perutz, *Organometallics.* 31 (2012) 1300–1314.
- [8] A. de Aguirre, S. Díez-González, F. Maseras, M. Martín, E. Sola, *Organometallics.* 37 (2018) 2645–2651.
- [9] S. Oldenhof, M. Lutz, J.I. van der Vlugt, J.N.H. Reek, *Chem. Commun.* 51 (2015) 15200–15203.
- [10] N.M. Leeb, M.W. Drover, J.A. Love, L.L. Schafer, J.M. Slattery, *Organometallics.* 37 (2018) 4630–4638.
- [11] M. Galiana-Cameo, A. Urriolabeitia, E. Barrenas, V. Passarelli, J.J. Pérez-Torrente, A. Di Giuseppe, V. Polo, R. Castarlenas, *ACS Catal.* 11 (2021) 7553–7567.
- [12] K. Saha, S. Kar, U. Kaur, T. Roisnel, S. Ghosh, *Organometallics.* 39 (2020) 4362–4371.
- [13] S. Gomosta, K. Saha, U. Kaur, K. Pathak, T. Roisnel, A.K. Phukan, S. Ghosh, *Inorg. Chem.* 58 (2019) 9992–9997.
- [14] K. Saha, B. Joseph, R. Borthakur, R. Ramalakshmi, T. Roisnel, S. Ghosh, *Polyhedron.* 125 (2017) 246–252.
- [15] R.S. Anju, B. Mondal, K. Saha, S. Panja, B. Varghese, S. Ghosh, *Chem. – A Eur. J.* 21 (2015) 11393–11400.
- [16] K. Saha, B. Joseph, R. Ramalakshmi, R.S. Anju, B. Varghese, S. Ghosh, *Chem. – A Eur. J.* 22 (2016) 7871–7878.
- [17] A.R. Cowley, A.L. Hector, A.F. Hill, A.J.P. White, D.J. Williams, J.D.E.T. Wilton-Ely, *Organometallics.* 26 (2007) 6114–6125.

- [18] P. Safari, S.A. Moggach, P.J. Low, *Dalton. Trans.* 49 (2020) 9835–9848.
- [19] E.C. Fitzgerald, A. Ladjarafi, N.J. Brown, D. Collison, K. Costuas, R. Edge, J.-F. Halet, F. Justaud, P.J. Low, H. Meghezzi, T. Roisnel, M.W. Whiteley, C. Lapinte, *Organometallics.* 30 (2011) 4180–4195.
- [20] M.A. Fox, B. Le Guennic, R.L. Roberts, D.A. Brue, D.S. Yufit, J.A.K. Howard, G. Manca, J.-F. Halet, F. Hartl, P.J. Low, *J. Am. Chem. Soc.* 133 (2011) 18433–18446.
- [21] S. Saha, A. Haridas, F. Assanar, C. Bansal, P.K. Sudhadevi Antharjanam, S. Ghosh, *Dalton. Trans.* 51 (2022) 4806–4813.
- [22] S. Takahashi, Y. Kuroyama, K. Sonogashira, N. Hagihara, *Chem. Informationsd.* 11 (1980) 627-630.
- [23] G.E. Ryschlewitsch, K.C. Nainan, S.R. Miller, L.J. Todd, W.J. Dewkett, M. Grace, H. Beall, M.F. Hawthorne, R. Leyden, *Inorg. Synth.* 15 (1974) 113–118.
- [24] These complexes have very low yield as they are highly sensitive and decomposition over time.
- [25] Gaussian 09, Revision C.01, M.J. Frisch, G.W. Trucks, H.B. Schlegel, G.E. Scuseria, M.A. Robb, J.R. Cheeseman, G. Scalmani, V. Barone, B. Mennucci, G.A. Petersson, H. Nakatsuji, M. Caricato, X. Li, H.P. Hratchian, A.F. Izmaylov, J. Bloino, G. Zheng, J.L. Sonnenberg, M. Hada, M. Ehara, K. Toyota, R. Fukuda, J. Hasegawa, M. Ishida, T. Nakajima, Y. Honda, O. Kitao, H. Nakai, T. Vreven, J.A. Montgomery, Jr., J.E. Peralta, F. Ogliaro, M. Bearpark, J.J. Heyd, E. Brothers, K.N. Kudin, V.N. Staroverov, T. Keith, R. Kobayashi, J. Normand, K. Raghavachari, A. Rendell, J.C. Burant, S.S. Iyengar, J. Tomasi, M. Cossi, N. Rega, J.M. Millam, M. Klene, J.E. Knox, J.B. Cross, V. Bakken, C. Adamo, J. Jaramillo, R. Gomperts, R.E. Stratmann, O. Yazyev, A.J. Austin, R. Cammi, C. Pomelli, J.W. Ochterski, R. L. Martin, K. Morokuma, V.G. Zakrzewski, G.A. Voth, P. Salvador, J.J. Dannenberg, S. Dapprich, A.D. Daniels, O. Farkas, J. B. Foresman, J.V. Ortiz, J. Cioslowski and D.J. Fox, Gaussian, Inc. Wallingford CT. (2010) 20–44.
- [26] A.D. Becke, *J. Chem. Phys.* 98 (1993) 5648–5652.
- [27] A.D. Becke, *Phys. Rev. A.* 38 (1988) 3098–3100.
- [28] C. Lee, W. Yang, R.G. Parr, *Matter Mater. Phys.* 37 (1988) 785–789.
- [29] F. Weigend, R. Ahlrichs, *Phys. Chem. Chem. Phys.* 7 (2005) 3297–3305.

- [30] Basis Set Exchange Library. <https://www.basissetexchange.org>.
- [31] F. London, *J. Phys. Radium*. 8 (1937) 397–409.
- [32] R. Ditchfield, *Mol. Phys.* 27 (1974) 789–807.
- [33] K. Wolinski, J.F. Hinton, P. Pulay, *J. Am. Chem. Soc.* 112 (1990) 8251–8260.
- [34] T. Onak, H. Landesman, R. Williams, I. Shapiro, *J. Phys. Chem.* 63 (1959) 1533–1535.
- [35] NBO Program 6.0, E.D. Glendening, J.K. Badenhoop, A.E. Reed, J.E. Carpenter, J.A. Bohmann, C.M. Morales, C.R. Landis, F. Weinhold, Theor. Chem. Institute, Univ. Wisconsin Madison, WI, USA. (2013).
- [36] K.B. Wiberg, *Tetrahedron*. 24 (1968) 1083–1096.
- [37] R.F.W. Bader, *Chem. Rev.* 91 (1991) 893–928.
- [38] R.F.W. Bader, *J. Phys. Chem. A*. 102 (1998) 7314–7323.
- [39] R.F.W. Bader, *A quantum theory*, Clarendon Oxford, UK. (1990).
- [40] T. Lu, F. Chen, Multiwfn: A multifunctional wavefunction analyzer. *J. Comput. Chem.* 33 (2012) 580–592.
- [41] Chemcraft - graphical software for visualization of quantum chemistry computations, <https://www.chemcraftprog.com>.
- [42] G. M. Sheldrick, SHELXS97 and SHELXL97, University of Gottingen: Germany, 1997.
- [43] G.M. Sheldrick, *Acta Cryst.* C71 (2015) 3–8.
- [44] O. V Dolomanov, L.J. Bourhis, R.J. Gildea, J.A.K. Howard, H. Puschmann, *J. Appl. Crystallogr.* 42 (2009) 339–341.
- [45] S. O. Pinheiro, J. R. de Sousa, M. O. Santiago, I. M. M. Carvalho, A. L. R. Silva, A. A. Batista, E. E. Castellano, J. Ellena Í. S. Moreira, I. C. N. Diógenes, *Inorg. Chem. Acta* 359 (2006) 391–400.
- [46] W. Diamantikos, H. Heinzelmann, E. Rath, H. Binder, *Zeitschrift für Anorg. und Allg. Chemie* 517 (1984) 111–117.

- [47] M.R.S.-J. Foreman, A.F. Hill, G.R. Owen, A.J.P. White, D.J. Williams, *Organometallics*. 22 (2003) 4446–4450.
- [48] L.Y. Goh, M.E. Teo, S.B. Khoo, W.K. Leong, J.J. Vittal, *J. Organomet. Chem.* 664 (2002) 161–169.
- [49] M.R.S.-J. Foreman, A.F. Hill, N. Tshabang, A.J.P. White, D.J. Williams, *Organometallics*. 22 (2003) 5593–5596.
- [50] P.J. Bailey, D.J. Lorono-Gonzales, C. McCormack, S. Parsons, M. Price, *Inorg. Chim. Acta.* 354 (2003) 61–67.
- [51] L.A. Graham, A.R. Fout, K.R. Kuehne, J.L. White, B. Mookherji, F.M. Marks, G.P.A. Yap, L.N. Zakharov, A.L. Rheingold, D. Rabinovich, *Dalton. Trans.* (2005) 171–180.
- [52] D.K. Roy, R. Borthakur, S. Bhattacharyya, V. Ramkumar, S. Ghosh, *J. Organomet. Chem.* 799–800 (2015) 132–137.

Entry for the Table of Contents



Reactivity of Cp* and borated-based κ^2 -N,S-chelated Ru(II) species with 1,4-diethynyl benzene has been demonstrated that led to the formation of hydrotrisborate ruthenium species and alkyne inserted ruthenium alkenyl complexes.